Flexible-fabricated sensor module with programmable magnetic actuators coupled to L-cysteine functionalized Ag@Fe 3 O 4 complexes for Cu 2+ detection in fish tissues

Kuiguo Han
Jiangsu University
Bin Jiang
Jiangsu University
Yanqun Tong
Jiangsu University
Wen Zhang (dr.wen.zhang@gmail.com)
Jiangsu University
Xiaobo Zou
Jiangsu University
Jiyong Shi
Jiangsu University
Xiaoyu Su
Jiangsu University

Research Article

Keywords: Electrochemical detection, Flexible-fabricated sensor, L-Cysteine, Ag@Fe3O4 nanowires

Posted Date: December 5th, 2022

DOI: https://doi.org/10.21203/rs.3.rs-2325152/v1

Additional Declarations: No competing interests reported.

Version of Record: A version of this preprint was published at Biomedical Microdevices on April 10th, 2023. See the published version at https://doi.org/10.1007/s10544-023-00654-2.

Abstract

Heavy metal contamination for seafood, particularly fish, is arising great concerns, and consequentially it is necessary to develop a simple and direct detection method. In this work, $Ag@Fe_3O_4$ is successfully prepared by simple solvothermal method, and we present a flexible-fabricated sensor module with assembled programmable magnetic actuators. The resulting sensor integrates a three-electrode system with two programmable magnetic actuators at the bottom of the device, which regulates the amount of current by adjusting the brake to control the adsorption force and vibration. The L-Cysteine functionalized $Ag@Fe_3O_4$ is coated on the surface of the electrode, then the Cu^{2+} is dropped into the reaction tank. Its performance is studied by cyclic voltammetry and electrochemical impedance spectroscopy, and the key experimental conditions such as deposition potential, deposition time, and electrolyte pH are gradually optimized. Under optimal conditions, Cu^{2+} can be detected over a wide linear range (0.01~4 μM) and at a low LOD (0.34 nM). The results show that the proposed method has a good application prospect in the detection of Cu^{2+}. This method is successfully applied to Cu^{2+} analysis in fish samples with an acceptable recovery of 93~102 %.

1. Introduction

Fish is rich in vitamins, proteins and other valuable nutrients, which are easily digested and absorbed by human body, therefore it is considered to be one of the most important food sources for global consumption(Khalili Tilami et al. 2018; Idowu et al. 2021). However, fish are frequently contaminated with heavy metals from sources such as domestic sewage and industrial wastewater(Shahjahan et al. 2022; Wang et al. 2020; Dallinger et al. 1987). As a representative heavy metal, Cu^{2+} in fish can be used as a reliable indicator of environmental pollution of water sources(Javed et al. 2019; Song et al. 2015). The concentration level of Cu^{2+} in human body directly affects human health, when Cu^{2+} content of the human body accumulates to a certain extent, it will cause serious harm to life and health, resulting in biochemical disorders, physiological dysfunction and various pathological changes in internal organs(Yu et al. 2021).

Various traditional detection techniques, such as inductively coupled plasma atomic emission spectrometry (ICP-AES)(Ebrahimi-Najafabadi et al. 2019), inductively coupled plasma mass spectrometry (ICP-MS)(Suo et al. 2019), and atomic absorption spectrometry(Ferreira et al. 2018) have been used to detect Cu^{2+}. However, these technologies are often complex, time-consuming, relatively expensive, and require bulky and non-portable devices. Electrochemical sensor has been recognized as a promising powerful tool for the determination of heavy metal ions due to its simplicity, low cost, portability, and high sensitivity. In electrochemical analysis, the accumulation of targets on the electrode surface facilitates the sensitivity of the response signal and the sensor(Jothimuthu et al. 2011; Shaik et al. 2021). Among them, magnetic separation is considered as an efficient separation-pre-concentration technology, which has the advantages of simple operation, high enrichment coefficient and wide application range(Kim et al. 2009a).

According to previous studies, the integration of magnetic nanoparticles (MNP) into sensors can improve the performance of the sensors(Rocha-Santos 2014). Fe_3O_4 magnetic nanoparticles have been widely used in the manufacture of biosensors due to their super paramagnetic, large specific area, and ease of preparation, which can be readily separated from the reaction mixture with a magnet and weighed immediately after removing the magnet new dispersion(Yuan et al. 2017; Guo et al. 2020). However, Fe_3O_4 still suffers from problems such as easy agglomeration of particles and oxidation in the process of application(Freitas et al. 2016). One-dimensional nanomaterials (wires, rods and tubes) have attracted widespread attention in electrochemical sensors due to their unique electrical, catalytic, physical, and chemical properties(Bi et al. 2008). Nanowire-based biosensors exhibit improved signal-to-noise ratios, fast electron transfer rates, enhanced sensitivity due to the rapid electron transfer between electrode and analyte(Qin et al. 2011). The stability of Fe_3O_4 under corrosive conditions was enhanced by combining silver nanowires (AgNWs) with Fe_3O_4.

In order to specifically identify Cu^{2+}, the surface of the composite material $Ag@Fe_3O_4$ nanowires (hereinafter collectively referred to as $Ag@Fe_3O_4$) must be functionally modified(Atapour et al. 2019). L-Cysteine (L-Cys) has been an important amino acid found in natural proteins that plays a key role in biological systems(Rohilla et al. 2020). The amino nitrogen and carboxyl oxygen in the L-Cys molecule have solitary pairs of electrons and can form stable coordination compounds with Cu^{2+}(Yang et al. 2001). The L-Cysteine molecule assembled on $Ag@Fe_3O_4$ surface through the Au-g bond (Betts et al. 2020). Traditional electrochemical sensors such as microfabrication techniques used in the semiconductor industry have matured due to their flexibility in the use of various materials and technologies to provide excellent control over sensor parameters. But manufacturing these sensors may require a variety of technologies and specialized facilities such as lithography and sputtering(Shamkhalichenar et al. 2020). As an alternative, flexible printed circuit technology offers various advantages such as flexibility, low manufacturing temperatures, and material savings(Li et al. 2020).

In this study, a facile polyol synthesis route is used to synthesize AgNWs by the reduction of $AgNO_3$ with ethylene glycol, and then the $Ag@Fe_3O_4$ nanocomposites are formed by loading Fe_3O_4 on silver nanowires by the solvothermal method. An analytical method for enriching Cu^{2+} traces using L-cysteine functionalized $Ag@Fe_3O_4$ nanocomposites is established, and L-Cys assembled on the surface of $Ag@Fe_3O_4$ through Ag-S bonds is able to capture Cu^{2+}. Flexible-fabricated sensor module is prepared, based on the technique of screen-printed circuit (FPC), to form an integrated three-electrode system. Meanwhile, the sensor module integrates a pair of programmable magnetic actuators for extensive analytical facilitations. The integrated design facilitates the miniaturization and systematization of the sensor and controls the current level by adjusting programmable magnetic actuators, thereby controlling the adsorption force. Under magnetic force, the L-Cys functionalized $Ag@Fe_3O_4$ is adsorbed directly onto the surface of the working electrode, and then the Cu^{2+} liquid is added, accelerating the adsorption of the Cu^{2+} liquid through the alternating magnetic field generated by the assembled programmable magnetic

actuators, while the programmable magnetic actuators vibrate under the action of the alternating magnetic field and can act as an alternative to stirring.

2. Experimentation

2.1 Reagents and Materials

Cu^{2+} standard solution (1000 μg/mL) was obtained the China Center for Standard Reference Materials. Polyvinylpyrrolidone (PVP) was purchased from Sigma-Aldrich. Hydrogen peroxide (30%), $AgNO_3$, Fe $(NO_3)_3 \cdot 9H_2O$, ethylene glycol, NaOH, diethylene glycol, and other chemical reagents were obtained from Sinopharm Chemical Reagent and were analytical grade and do not require further purification. Deionized water was produced using the Milli-Q system (USA) throughout the experiment.

2.2 Characterization instruments

The microstructure of the composites was observed using transmission electron microscopy (TEM, JEM-2100, JEOL, Japan) and scanning electron microscopy (SEM, JSM-7800M, JEOL, Japan). The elemental composition was explored using energy dispersive spectroscopy (EDS, Octane SDD, AMETEK, USA). X-ray diffractometer (XRD, D8 ADVANCE, Bruker, Germany) was adopted to explore crystal phases of AgNWs and Ag@Fe_3O_4, at 2θ angle from 10° to 80° with a Cu-Kα radiation source (λ = 1.5405 Å). Synthesis of AgNWs and Ag@Fe_3O_4 were examined with UV–Vis absorption spectra (UV-2600, Shimadzu, Japan) in a window of 300–500 nm, the Cu^{2+} in fish was explored using inductively coupled plasma mass spectrometry (ICP-MS, X series II, America).

2.3 Synthesis of L-Cys/Ag@Fe_3O_4 composites

AgNWs was synthesized by reducing $AgNO_3$ with ethylene glycol by polyol method(Fahad et al. 2019). Briefly, 20 mL of ethylene glycol was heated first in an oil bath at 150°C for 1 hour, then 5 mL of $AgNO_3$-ethylene glycol solution (containing 0.24 mol $AgNO_3$ in ethylene glycol) and 5 mL of PVP-ethylene glycol solution (containing 0.24 mol PVP in ethylene glycol) were added drop by drop. The solution became turbid and grey in about 15 min, indicating the appearance of silver nanowires, and continued to reflect at 150°C for 5 hours, leaving a grey precipitate at the end of the reaction. Finally, the solution was washed 3 ~ 5 times with ethanol and acetone and dried at 60°C for 10 ~ 12 hours.

The AgNWs (0.1 mmol) and Fe $(NO_3)_3$ (0.4 mmol) were first dissolved in 10 mL of diethylene glycol, then sodium acetate (0.01 mol) and 3 mL of ethylene glycol were added in turn to obtain an orange-brown solution. Then, resulting mixture was transferred to a 20 mL PTFE-lined stainless-steel autoclave, which was sealed and kept at 200°C for 10 hours. The autoclave was cooled naturally to room temperature. The precipitate Ag@Fe_3O_4 was washed 3 times with distilled water and ethanol and dried at 30°C for 6 h. Finally, the product was dispersed in ethanol and stored at room temperature for further characterization. In addition, pure Fe_3O_4 nanoparticles were fabricated as a comparative test.

L-Cys can bind to Ag@Fe_3O_4 nanowires through Ag-S bonds. 10 mmol L-Cys solution was prepared for experimental use. The prepared L-Cys solution and Ag@Fe_3O_4 nanowires were first mixed in a beaker and incubated for about 30 min. The L-Cys/Ag@Fe_3O_4 composites were collected by magnet adsorption. Finally, the composites were rinsed with deionized water to remove the incompletely bound L-Cys.

2.4 Manufacture of flexible sensors

Sensor module was prepared based on our well-establish technique(Su et al. 2022) but with innovated magnetic actuator integration (Fig. 1A). Briefly, the module was initially fabricated on 0.2 mm flexible polyimide substrate using FPC technique. All pads on the top layer, as semi-finished electrodes, were made with 17 μm Cu film and covered with 0.5 μm Au. The semicircular pad was directly adopted as counter electrode. The arc one was subject to Ag/AgCl paste coating to organize functional reference electrode. The central round pad (diameter = 4 mm) was adopted as working electrode until further modification. Meanwhile, a pair of E-shape Mn-Zn ferrites (Type: EE10, μ > 10000) were commercially purchased. By assembling windings (N = 600, with 0.08 mm varnished wire) to each of them, the magnetic actuators were well obtained. These magnetic actuators were glued on the bottom of the sensor module with tiny magnetic gap as 0.5 mm, and sealed with moisture-resisted epoxy. Thus, they could accept external AC or DC excitation (0 ~ 1 V) for desired performance (Fig. 1B C).

Synchronously, two independent pad groups were fabricated onto the bottom of the SPE, well forming the dual electricfield driver. Area distribution for each electricfield unit could be trimmed by assembling bypass resistors. During operation, external excitation was applied to this programmable electricfield driver and the working electrode.

2.5 Sensor modification and electrochemical measurement

Electrochemical experiments were performed using the CHI-660D analyzer (CH Instruments, China). Cyclic voltammetry (CV) and electrochemical impedance spectroscopy (EIS) were tested for 5 mM $K_3[Fe(CN)_6]$ and 0.1 M KCl, respectively. In CVs, the scanning period and potential window was 1 V and − 0.2 ~ 0.6 V. The frequency range and amplitude of EIS were set as 10^{-2}~10^5 Hz, and 5 mV.

Previous studies had reported that Cu^{2+} can be stably bound to the amino nitrogen and carboxyl oxygen in L-Cys. The prepared L-Cys/Ag@Fe_3O_4 composite was homogeneously dropped onto the screen-printed electrode (SPE), and the solution of Cu^{2+} was incubated on the surface for 30 minutes by adsorbing it onto the surface of SPE through the electromagnet below (Figure. 1D). After incubation and natural drying the surface is rinsed with deionized water.

Cu^{2+} was determined by differential pulse adsorption solvation voltammetry (DPAdSV)(Fu et al. 2013). 10 mL of PBS (0.1 mol L^{-1}) was dropped into the reaction tank. DPAdSV scanned the working electrode over a range of -0.4 to 0.6 V. At -0.4 V, Cu^{2+} was reduced to metallic Cu.

2.6 Sample pretreatment

Fish samples were purchased from the local market, and the muscle was separated, cut into small pieces and rinsed three times with deionized water. Place 1 g of dried sample in the digestion vessel and add 10 mL of HNO_3 (70%) and 12 mL of H_2O_2 (30%). The vessel was immediately assembled and placed in a 150°C microwave digester for approximately 5 hours. After complete digestion of the sample, the solution was cooled to room temperature and the pH of the digestion solution was adjusted to neutral, the liquid fraction was separated and dried under vacuum to 1 mL. Finally, the resulting solid was dissolved in 1 mL of deionized water and supplemented with 0.1 mol L^{-1} of citric acid and sodium citrate buffer. The prepared solution was stored in a refrigerator at 4°C in preparation for further determination.

3. Results And Discussion

3.1 Characterization of Ag@Fe_3O_4

The AgNWs and Ag@Fe_3O_4 were characterized with SEM to observe the morphology of the synthesized materials. Figure. 2A and B showed typical SEM images of the prepared AgNWs, and it could be seen that the AgNWs have a relatively smooth surface and with random arrangements. The length of AgNWs was in the range of 40 ~ 60 μm, and the diameter was about 200 nm. The typical diameter of Ag@Fe_3O_4 nanowires was about 200 nm, the length was similar to that of AgNWs, and the surface of AgNWs was coated with Fe_3O_4 (Figure. 2C). Figure. 2D showed a schematic diagram of Ag@Fe_3O_4 subjected to magnetic adsorption. EDS spectra were employed to illustrate elemental compositions of AgNWs and Ag@Fe_3O_4. In Fig. 2E, Ag element was distinctly observed in AgNWs spectrum, and after the addition of Fe_3O_4, the content of Ag element decreased significantly and the content of C and Fe increased.

Crystal structures of AgNWs and Ag@Fe_3O_4 were investigated with XRD. As shown in Figure. 2F, the XRD spectrum of AgNWs appeared at 38.2°, 43.6°, 64.2°, and 77.1°, corresponding to the face-centered cubic Ag (JCPDS, No. 04-0783) (Chen et al. 2014)(111), (200), (220), and (311) crystal planes. The strong diffraction peak proved that the prepared silver nanowires have a good crystal structure. Some weakly diffractive peaks were attributed to Fe_3O_4 (JCPDS No. 19–0629)(Iyengar et al. 2014), such as the two peaks at 35.6°and 57.2°, corresponding to the diffraction peaks of (311) and (511). Thus, XRD spectra confirmed that AgNWs was successfully loaded onto Fe_3O_4.

UV–vis spectra of Fe_3O_4 and Ag@Fe_3O_4 were tested with Ultraviolet–visible Spectrophotometer (Figure. 2G). Ag@Fe_3O_4had no absorption peaks in the UV-Vis spectrum. However, AgNWs presented a distinct absorption peak at 380 nm, which may be due to the surface plasmon resonance of AgNWs.

3.2 Electrochemical characterization

The electrochemical behavior of bare SPE, Ag@Fe_3O_4/SPE and L-Cys/Ag@Fe_3O_4/SPE were compared with CV in 0.5 mol L^{-1} NaOH.Symmetrical shapes and reversible redox peaks were observed on bare SPE as shown in Figure. 3A. The modification with Fe_3O_4 showed a significant increase in peak current, which

was related to the good electrocatalytic properties of Fe_3O_4, as their electrical properties and adsorption ability could effectively facilitate the electron transfer between the solution and electrode interfaces. The peak currents of Ag@Fe_3O_4/SPE were further enhanced by the addition of AgNWs. The redox peak decreased after L-Cys incubation, which was caused by cysteine insulation(Cheng et al. 2016).

EIS was considered to be an effective tool for probing the interfacial properties of surface-modified electrodes. In a typical EIS, the diameter of the semicircle is equal to the electron transfer resistance (Ret), which reflected the electron transfer kinetics of the redox probe at the electrode surface. As shown in Figure. 3B, the Ret value of Ag@Fe_3O_4/SPE was much higher than that of bare SPE, which is due to the fact that Fe_3O_4 is a poorly conductive metal oxide with a large electron transfer impedance, as such while AgNWs were able to accelerate the electron transfer on the electrode surface and reduce the electron transfer resistance. After modifying AgNWs@Fe_3O_4 with L-cysteine, the Ret value of L-cysteine/Ag@Fe_3O_4/SPE was lower than that of Ag@Fe_3O_4/SPE because L-cysteine can provide tunable conductivity and fast electron transfer(Moccelini et al. 2008).

To explore the potential analytical benefits of benefiting from Ag@Fe_3O_4, bare SPE, Fe_3O_4/SPE and Ag@Fe_3O_4/SPE were used for CV analysis (Figure. 3C). Then, calculated the electroactive area of these electrodes according to the Randles-Sevcik equation(Su et al. 2022):

$$Ip = (2.69 \times 10^5) A D^{\frac{1}{2}} c v^{\frac{1}{2}}$$

where *Ip* was the peak current, *A* was the active area of the electrode, *D* and *c* were the diffusion coefficients and K_3 [Fe $(CN)_6$] concentration, *v* was the pre-stabilized scan rate. For bare SPE, Fe_3O_4/SPE and Ag@Fe_3O_4/SPE, which respectively had an electroactive area of 0.040, 0.055 and 0.065 cm^2(Figure. 3D). It illustrated that Ag@Fe_3O_4/SPE presented much larger electroactive area than bare SPE or Fe_3O_4/SPE.

3.3 Optimization of experimental parameters

For best performance, key parameters such as deposition potential, deposition time, electrolyte pH, incubation time, driving voltage, and magnetic field frequency were optimized to maximize the efficiency and sensitivity of the electrode.

The effect of deposition potential on current was studied over a potential range of -1.5 V to -1 V. As shown in Figure. 4A, with the deposition potential decreases from − 1.5 V to -1.2 V, the peak current gradually increases until − 1.2 V. At higher potentials, the peak intensity of the peeling current decreases, which is caused by hydrogen reduction on the surface of the modified electrode. Therefore, the − 1.2 V potential was optimal for detecting Cu^{2+}.

The response current raised rapidly with the peel time between 30 ~ 120 s, and did not change much after 120 s (Figure. 4B), the peel signal peaks within 120 s, indicating that the electrode surface had reached

the maximum load capacity, and the extended deposition time led to the loss of the peel current strength. Therefore, 120 s was chosen for this experiment.

The selection of the appropriate pH was also crucial, as pH affects the sensitivity and selectivity of quantitative studies. Therefore, the voltametric signal of Cu^{2+} was examined in PBS over the pH range from 3 to 9. Figure. 4C showed the peak current versus electrolyte pH. The peak current increased with increasing pH from 2 to 5 and the maximum peak current was observed at pH = 5. It is possible that when the pH is small (< 5), competition and repulsion affect the binding effect of Cu^{2+} to L-Cys, while when pH > 5, the interaction between the amino nitrogen in L-Cys and AgNWs was enhanced, thus weakening the linkage of the amino group to Cu^{2+}.

L-Cys was assembled on the Ag@Fe_3O_4 surface via Ag-S bond. the amount of L-Cys binding on the Ag@Fe_3O_4 surface was dependent on the incubation time. As shown in Figure. 4D, the peak current increased significantly with the incubation time up to 30 mins and maintained a stable response after 30 min. This may be due to the increase in the amount of L-Cys binding on the Ag@Fe_3O_4 surface from 1 min to 30 min during which the amount of trapped Cu^{2+} also increased, saturation was reached after about 30 min.

Both the drive voltage (which provides the excitation source for the magnetic brake to operate) and the magnetic field frequency of the magnetic brake also affected the peak current, because the vibrational effect provided by the magnetic brake played an important role in the incubation process. As could be seen in Figure. 4E, when the drive voltage was set at 0 ~ 0.6 V, the peak current increased rapidly, but with higher voltages the vibrations became more intense and many bubbles form in the sample solution, impeding the transfer of mass at the sensing interface and causing the peak current to decay. Similarly, as the magnetic field frequency increased(Figure.4F), the number of discharges per unit time increased and the peak current tended to increase rapidly, however, when the frequency was set too exorbitant, it was conjectured that the brake temperature increased due to the increase in average discharge energy per unit time, affecting the binding of L-Cys to Ag@Fe_3O_4.

3.4 L-Cys/Ag@Fe3O4/SPE performance analysis

The analytical performance of L-Cys/Ag@Fe_3O_4/SPE for Cu^{2+} detection was investigated under optimized conditions. As shown in Figure. 5A and B, the concentration of Cu^{2+} was linear in the range of 0.01 ~ 4 μM. The linear regression equation for the analytical current with Cu^{2+} concentration was Ip (μA) = 0.064C (μM) + 2.169 (R^2 = 0.992), where Ip represented the peak current and C represented the concentration of Cu^{2+} (mol L^{-1}). The sensitivity for Cu^{2+} detection was 0.064 μA/(μM), and the limit of detection (LOD) was 0.34 μgL^{-1}. LOD was defined as LOD = 3Sb/S, where Sb and S are the standard deviation of 10 blank signals and the slope of the calibration curve. Compared with previously reported electrochemical electrodes for Cu^{2+}, it could be seen that the proposed L-Cys/Ag@Fe_3O_4/SPE presented low detection limit, high sensitivity, and simple synthesis (Table 1).

3.5 Interference, repeatability, long-term stability

A number of interfering metal ions were detected under the same optimized conditions, including 10 μM (10 folds of Cu^{2+}) Zn^{2+}, Pb^{2+}, Mg^{2+}, K^{+}, Na^{+}, Ca^{2+}, Hg^{2+}, Cd^{2+}, and Ni^{2+}. As shown in Figure. 5C, the responses of these interfering ions were very small at such high concentrations. In order to further confirm the interfering nature of the other ions, the relatively strongly interfering ions, 100 μM Hg^{2+}, Pb^{2+}, Ca^{2+} and Cd^{2+} (100 folds of Cu^{2+}) were investigated (Figure. 5D), and the responses of these interfering ions remained small at such high concentrations. Therefore, it indicated that these ions do not interfere with the determination of Cu^{2+}. This is because Cu^{2+} has stronger coordination with L-Cys compared to other metal ions and forms stable complexes under the same conditions.

The reproducibility and stability of L-Cys/Ag@Fe_3O_4/SPE were investigated by continuous cycling electrodes. As shown in Figure. 5E, the relative standard deviation (RSD) is 2.360%, which confirmed L-Cys/Ag@Fe_3O_4/SPE is stable and reproducible for Cu^{2+} detection.

Storage stability was studied by measuring the DPADSV response to Cu^{2+} every two days for 15 days, and compared the peak current on the first and last days, it was found to decrease slowly, from 3.6 μA on the first day to 3.16 μA, maintaining 88% of the initial response. It is shown that L-Cys/Ag@Fe_3O_4/SPE has good storage stability (Figure. 5F).

Table 1
Comparison of the L-Cys/Ag@Fe_3O_4/SPE and the other methods for the determination of Cu^{2+}.

Detection method	Materials	LOD (nM)	Linear ranges (μM)	Ref
Fluorescence	Coumarin 334	87	0—0.8	(Kim et al. 2009b)
Fluorescence	DA 1	89	0—10	(Cho et al. 2019)
UV–vis	PPV@MSN@CdTe	31.2	0.03—0.16	(Sha et al. 2015)
UV–vis	TiO_2-TAP	2.51	0.01—125	(Ghasemi et al. 2020)
Electrochemistry	NiO/MoO_3/CS	5.69	0—25	(Shang et al. 2019)
Electrochemistry	Ni/NiO/ZnO-6/CS	0.81	0—6	(Yu et al. 2021)
Electrochemistry	rGO-SbNPs	34.1	0.1—4.5	(Silva et al. 2022)
Electrochemistry	L-Cys/Ag@Fe_3O_4 /SPE	0.34	0.01—4	This work

3. 6 Electrochemical Detections Of Cu In Fish

The performance of L-Cys/Ag@Fe_3O_4/SPE for practical applications was evaluated by analyzing fish samples. To verify the accuracy and reliability of the method, three sets of breams, grass carp and black carp sample extracts were prepared for DPAdSV and ICP-MS based assays, respectively. As shown in Table 2, the results of DPAdSV assay were compared with those of ICP-MS with error rates in the range of 3.7 ~ 9.3%. In addition, 0.5 μM, 1 μM and 4 μM of Cu^{2+} were added to three groups of fish samples and analyzed using DPAdSV with recoveries in the range of 93 ~ 102% and relative standard deviations (RSD) < 6.6%. These results indicated that L-Cys/Ag@Fe_3O_4 /SPE is suitable for Cu^{2+} determination with excellent accuracy, precision and reliability in the analysis of natural samples, and showed good applicability for the determination of real samples.

Table 2
Analyses of Cu^{2+} in fish samples.

Sample	Method comparison			Recovery test of DPAdSV		
	This method (μM)	ICP-MS (μM)	|Error| (%)	Added (μM)	DPADSV (μM)	Recovery (%)
Bream 1	0.17 ± 0.01	0.18 ± 0.02	5.6	0.5	0. 47 ± 0.03	94
Grass carp 1	0.11 ± 0.03	0.12 ± 0.03	8.3	0.5	0. 48 ± 0.02	96
Black carp 1	0.19 ± 0.01	0.18 ± 0.02	5.6	0.5	0. 51 ± 0.02	102
Bream 2	0. 35 ± 0.02	0. 32 ± 0.01	9.3	1	0.93 ± 0.05	93
Grass carp 2	0.81 ± 0.02	0.78 ± 0.03	3.8	1	0.96 ± 0.04	96
Black carp 2	0.44 ± 0.03	0.47 ± 0.02	6.4	1	0.95 ± 0.02	95
Bream 3	1.18 ± 0.04	1.24 ± 0.01	4.8	4	3.93 ± 0.02	98.3
Grass carp 3	2.13 ± 0.03	2.05 ± 0.02	3.9	4	3.87 ± 0.03	96.8
Black carp 3	1.84 ± 0.02	1.91 ± 0.02	3.7	4	4.03 ± 0.02	101

4. Conclusion

In this study, we successfully synthesize Ag@Fe_3O_4 composites using a solvothermal method, establish an analytical method for the trace enrichment of Cu^{2+} using L-Cys-functionalized Ag@Fe_3O_4 composites. Furthermore, we introduce a flexible-fabricated sensor module with assembled programmable magnetic actuators for the differential pulse adsorption solvation voltammetry of Cu^{2+} in fish samples. Compared with previously reported methods for electrochemical determination of Cu^{2+}, this method has the advantages of simple fabrication, low detection limit (0.34 nM), excellent anti-interference, and low cost inexpensive. Under optimal conditions, the detection of Cu^{2+} showed good linearity in a wide linear range

(0.01 ~ 4 μM). In the analysis of fish samples, the recoveries range from 93–96.8% with excellent accuracy, precision and reliability, and show good applicability for the determination of real samples.

Declarations

Acknowledges

This work was supported by National Natural Science Foundation of China (32102080, 31801631, 31671844, 1601360061); Natural Science Foundation of Jiangsu Province (BK20160506, BK20180865); Post-graduate Research & Practice Innovation Program of Jiangsu Province (KYCX21_3395).

Conflict of interest The authors declare that they have no conflict of interest.

References

1. S. Khalili Tilami, S. Sampels,Nutritional Value of Fish: Lipids, Proteins, Vitamins, and Minerals. Reviews in Fisheries Science & Aquaculture. **26**(2), 243–253 (2018)
2. A.T. Idowu, O.O. Igiehon, S. Idowu, O.O. Olatunde, S. Benjakul,Bioactivity Potentials and General Applications of Fish Protein Hydrolysates. Int. J. Pept. Res. Ther. **27**(1), 109–118 (2021)
3. M. Shahjahan, K. Taslima, M.S. Rahman, M. Al-Emran, S.I. Alam, C. Faggio,Effects of heavy metals on fish physiology – A review. Chemosphere. **300**, 134519 (2022)
4. J. Wang, Q. Shan, X. Liang, F. Guan, Z. Zhang, H. Huang, H. Fang,Levels and human health risk assessments of heavy metals in fish tissue obtained from the agricultural heritage rice-fish-farming system in China. J. Hazard. Mater. **386**, 121627 (2020)
5. R. Dallinger, F. Prosi, H. Segner, H. Back,Contaminated food and uptake of heavy metals by fish: a review and a proposal for further research. Oecologia. **73**(1), 91–98 (1987)
6. M. Javed, N. Usmani,An Overview of the Adverse Effects of Heavy Metal Contamination on Fish Health. Proceedings of the National Academy of Sciences, India Section B: Biological Sciences. **89**(2), 389–403(2019)
7. L. Song, M.G. Vijver, W.J.G.M. Peijnenburg, T.S. Galloway, C.R. Tyler,A comparative analysis on the in vivo toxicity of copper nanoparticles in three species of freshwater fish. Chemosphere. **139**, 181–189 (2015)
8. J. Yu, X. Zhang, M. Zhao, Y. Ding, Z. Li, Y. Ma, H. Li, H. Cui,Fabrication of the Ni-based composite wires for electrochemical detection of copper(II) ions. Anal. Chim. Acta **1143**, 45–52 (2021)
9. H. Ebrahimi-Najafabadi, A. Pasdaran, R. Rezaei Bezenjani, E. Bozorgzadeh,Determination of toxic heavy metals in rice samples using ultrasound assisted emulsification microextraction combined with inductively coupled plasma optical emission spectroscopy. Food Chem. **289**, 26–32 (2019)
10. L. Suo, X. Dong, X. Gao, J. Xu, Z. Huang, J. Ye, X. Lu, L. Zhao,Silica-coated magnetic graphene oxide nanocomposite based magnetic solid phase extraction of trace amounts of heavy metals in water

samples prior to determination by inductively coupled plasma mass spectrometry. Microchemical J. **149**, 104039 (2019)

11. S.L.C. Ferreira, M.A. Bezerra, A.S. Santos, W.N.L. dos Santos, C.G. Novaes, O.M.C. de Oliveira, M.L. Oliveira, R.L. Garcia,Atomic absorption spectrometry – A multi element technique. TrAC Trends in Analytical Chemistry. **100**, 1–6 (2018)
12. P. Jothimuthu, R.A. Wilson, J. Herren, E.N. Haynes, W.R. Heineman, I. Papautsky,Lab-on-a-chip sensor for detection of highly electronegative heavy metals by anodic stripping voltammetry. Biomedical Microdevices. **13**(4), 695–703 (2011)
13. S. Shaik, A. Saminathan, D. Sharma, J.A. Krishnaswamy, D.R. Mahapatra,Monitoring microbial growth on a microfluidic lab-on-chip with electrochemical impedance spectroscopic technique. Biomedical Microdevices. **23**(2), 26 (2021)
14. J.A. Kim, H.J. Lee, H.-J. Kang, T.H. Park,The targeting of endothelial progenitor cells to a specific location within a microfluidic channel using magnetic nanoparticles. Biomedical Microdevices. **11**(1), 287–296 (2009a)
15. T.A.P. Rocha-Santos, Sensors and biosensors based on magnetic nanoparticles. TrAC Trends in Analytical Chemistry. **62**, 28–36 (2014)
16. Y. Yuan, S. Li, Y. Xue, J. Liang, L. Cui, Q. Li, S. Zhou, Y. Huang, G. Li, Y. Zhao, A Fe3O4@Au-basedpseudo-homogeneous electrochemical immunosensor for AFP measurement using AFP antibody-GNPs-HRP as detection probe. Anal. Biochem. **534**, 56–63 (2017)
17. W. Guo, A. Umar, M.A. Alsaiari, L. Wang, M. Pei, Ultrasensitive and selective label-free aptasensor for the detection of penicillin based on nanoporous PtTi/graphene oxide-Fe3O4/ MWCNT-Fe3O4 nanocomposite. Microchemical J. **158**, 105270 (2020)
18. M. Freitas, M. Sá Couto, M.F. Barroso, C. Pereira, N. de-los-Santos-Álvarez, A.J. Miranda-Ordieres, M.J. Lobo-Castañón, C. Delerue-Matos,Highly Monodisperse Fe3O4@Au Superparamagnetic Nanoparticles as Reproducible Platform for Genosensing Genetically Modified Organisms. ACS Sens. **1**(8), 1044–1053 (2016)
19. Y. Bi, G. Lu, Facile Synthesis of Platinum Nanofiber/Nanotube Junction Structures at Room Temperature. Chem. Mater. **20**(4), 1224–1226 (2008)
20. X. Qin, H. Wang, Z. Miao, X. Wang, Y. Fang, Q. Chen, X. Shao,Synthesis of silver nanowires and their applications in the electrochemical detection of halide. Talanta. **84**(3), 673–678 (2011)
21. M. Atapour, G. Amoabediny, M.J.R.a. Ahmadzadeh-Raji,Integrated optical and electrochemical detection of Cu 2 + ions in water using a sandwich amino acid–gold nanoparticle-based nano-biosensor consisting of a transparent-conductive platform **9**(16), 8882–8893(2019)
22. D. Rohilla, S. Chaudhary, N. Kaur, A. Shanavas, Dopamine functionalized CuO nanoparticles: A high valued “turn on” colorimetric biosensor for detecting cysteine in human serum and urine samples. Mater. Sci. Engineering: C **110**, 110724 (2020)
23. W. Yang, J. Justin Gooding, D. Brynn Hibbert,Characterisation of gold electrodes modified with self-assembled monolayers of l-cysteine for the adsorptive stripping analysis of copper. J. Electroanal.

Chem. **516**(1), 10–16 (2001)

24. H.D. Betts, O.M. Linder-Patton, C.J. Sumby, 2020. A Stable Coordination Polymer Based on Rod-Like Silver(I) Nodes with Contiguous Ag-S Bonding. Molecules
25. H. Shamkhalichenar, C.J. Bueche, J.-W. Choi, 2020. Printed Circuit Board (PCB) Technology for Electrochemical Sensors and Sensing Platforms. Biosensors
26. X. Li, M. Zhang, Y. Hu, J. Xu, D. Sun, T. Hu, Z. Ni,Developing a versatile electrochemical platform with optimized electrode configuration through screen-printing technology toward glucose detection. Biomedical Microdevices. **22**(4), 74 (2020)
27. S. Fahad, H. Yu, L. Wang, A. Zain ul, M. Haroon, R.S. Ullah, A. Nazir, K.-u-R. Naveed, T. Elshaarani, A. Khan,Recent progress in the synthesis of silver nanowires and their role as conducting materials. J. Mater. Sci. **54**(2), 997–1035 (2019)
28. X. Su, H. Wang, C. Wang, X. Zhou, X. Zou, W. Zhang, Programmable dual-electric-field immunosensor using MXene-Au-based competitive signal probe for natural parathion-methyl detection. Biosens. Bioelectron. **214**, 114546 (2022)
29. X.-C. Fu, J. Wu, J. Li, C.-G. Xie, Y.-S. Liu, Y. Zhong, J.-H. Liu,Electrochemical determination of trace copper(II) with enhanced sensitivity and selectivity by gold nanoparticle/single-wall carbon nanotube hybrids containing three-dimensional l-cysteine molecular adapters. Sens. Actuators B: Chem. **182**, 382–389 (2013)
30. J. Chen, Y. Liu, G. Zhu, A. Yuan, Ag@Fe3O4 nanowire: fabrication, characterization and peroxidase-like activity. Cryst. Res. Technol. **49**(5), 309–314 (2014)
31. S.J. Iyengar, M. Joy, C.K. Ghosh, S. Dey, R.K. Kotnala, S.J.R.a. Ghosh,Magnetic, X-ray and Mössbauer studies on magnetite/maghemite. core–shell Nanostruct. fabricated through aqueous route **4**(110), 64919–64929 (2014)
32. Y. Cheng, H. Fa, W. Yin, C. Hou, D. Huo, F. Liu, Y. Zhang, C. Chen, A sensitive electrochemical sensor for lead based on gold nanoparticles/nitrogen-doped graphene composites functionalized with l-cysteine-modified electrode. J. Solid State Electrochem. **20**(2), 327–335 (2016)
33. S.K. Moccelini, S.C. Fernandes, I.C. Vieira,Bean sprout peroxidase biosensor based on l-cysteine self-assembled monolayer for the determination of dopamine. Sens. Actuators B: Chem. **133**(2), 364–369 (2008)
34. M.H. Kim, H.H. Jang, S. Yi, S.-K. Chang, M.S. Han,Coumarin-derivative-based off–on catalytic chemodosimeter for Cu2 + ions. Chemical Communications.(32), 4838–4840(2009b)
35. S.W. Cho, A.S. Rao, S. Bhunia, Y.J. Reo, S. Singha, K.H. Ahn,Ratiometric fluorescence detection of Cu(II) with a keto-dipicolylamine ligand: A mechanistic implication. Sens. Actuators B: Chem. **279**, 204–212 (2019)
36. J. Sha, C. Tong, H. Zhang, L. Feng, B. Liu, C. Lü,CdTe QDs functionalized mesoporous silica nanoparticles loaded with conjugated polymers: A facile sensing platform for cupric (II) ion detection in water through FRET. Dyes and Pigments. **113**, 102–109 (2015)

37. Z. Ghasemi, A. Mohammadi, Sensitive and selective colorimetric detection of Cu (II) in water samples by thiazolylazopyrimidine-functionalized TiO2 nanoparticles. Spectrochimica Acta Part A: Molecular and Biomolecular Spectroscopy. **239**, 118554 (2020)
38. J. Shang, M. Zhao, H. Qu, H. Li, R. Gao, S. Chen, New application of p-n junction in electrochemical detection: The detection of heavy metal ions. J. Electroanal. Chem. **855**, 113624 (2019)
39. M.K.L. Silva, I. Cesarino,Electrochemical sensor based on Sb nanoparticles/reduced graphene oxide for heavy metal determination. Int. J. Environ. Anal. Chem. **102**(13), 3109–3123 (2022)

Figures

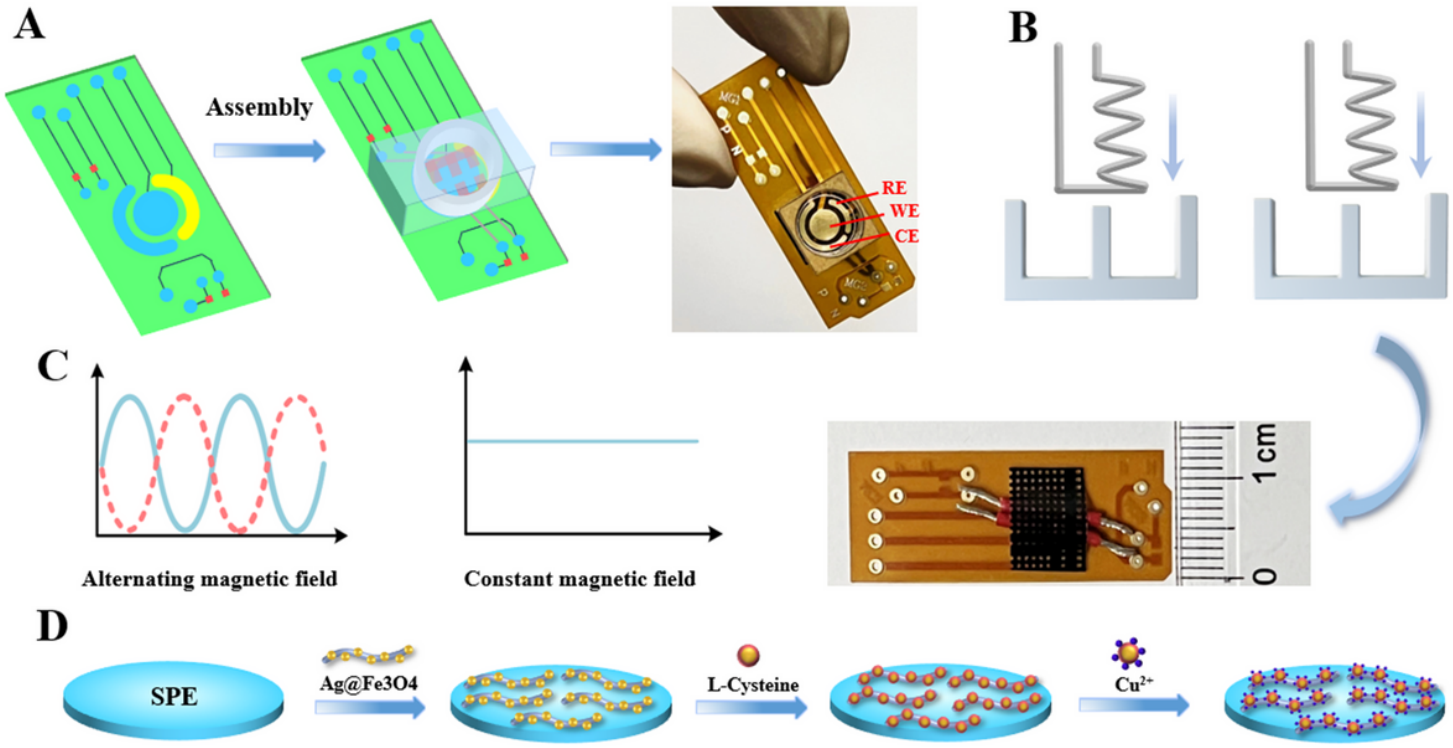

Figure 1

(A) schematic diagram of sensor fabrication, (B) prototype sensor module, (C) assembly of magnetic field effect of electromagnet, (D) complex modification of $Ag@Fe_3O_4$, L-cysteine and Cu^{2+} assembled on the fabricated sensor module.

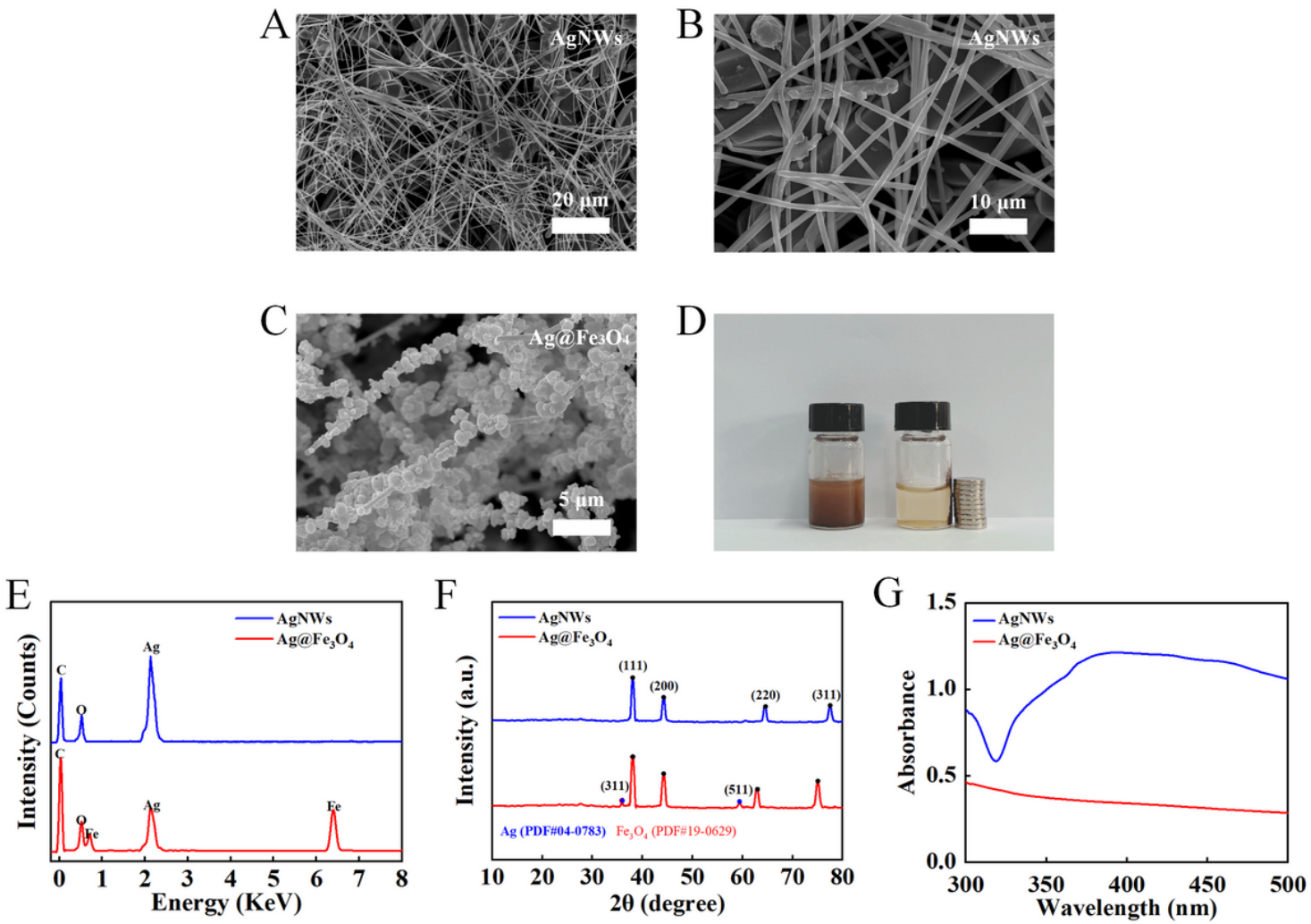

Figure 2

(A) SEM plots of AgNWs: 20 μm, (B)10 μm, (C) SEM plots of $Ag@Fe_3O_4$, (D) Schematic diagram of magnetic adsorption of $Ag@Fe_3O_4$, (E) AgNWs and $Ag@Fe_3O_4$ EDS spectroscopy, (F) XRD spectra of AgNWs and $Ag@Fe_3O_4$, (G) UV-Vis spectra of AgNWs and $Ag@Fe_3O_4$.

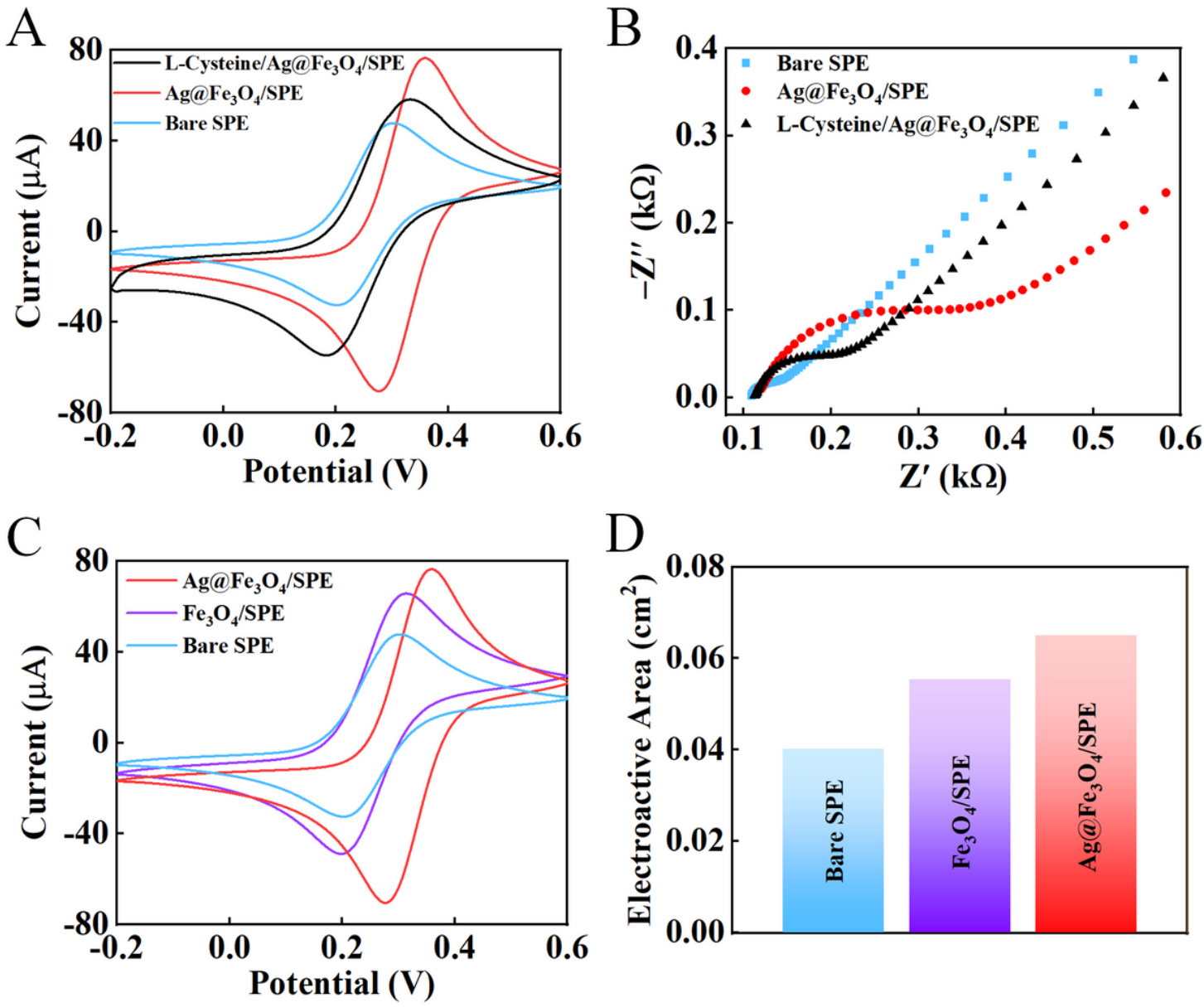

Figure 3

(A) CV and (B) EIS curves, including bare SPE, Ag@Fe_3O_4/SPE, L-Cys/Fe_3O_4/SPE different modifications are well captured, (C) CV curves and (D) electroactive region of bare SPE, Fe_3O_4/SPE and Ag@Fe_3O_4/SPE.

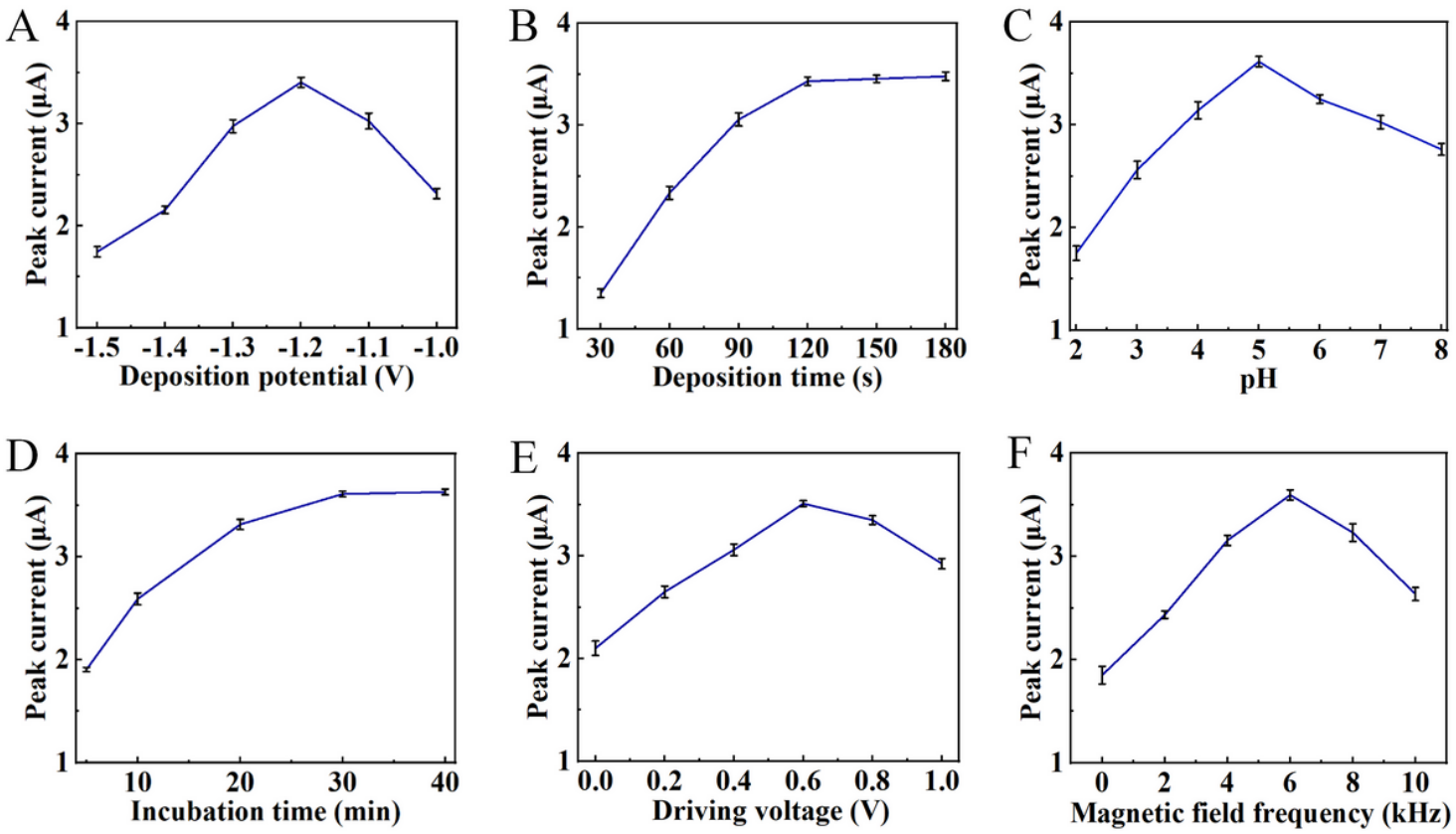

Figure 4

Optimized conditions for detecting 10 μM Cu^{2+} include: (A) deposition potential, (B) deposition time, (C) electrolyte pH and (D) incubation time, (E) driving voltage and (F) magnetic field frequency.

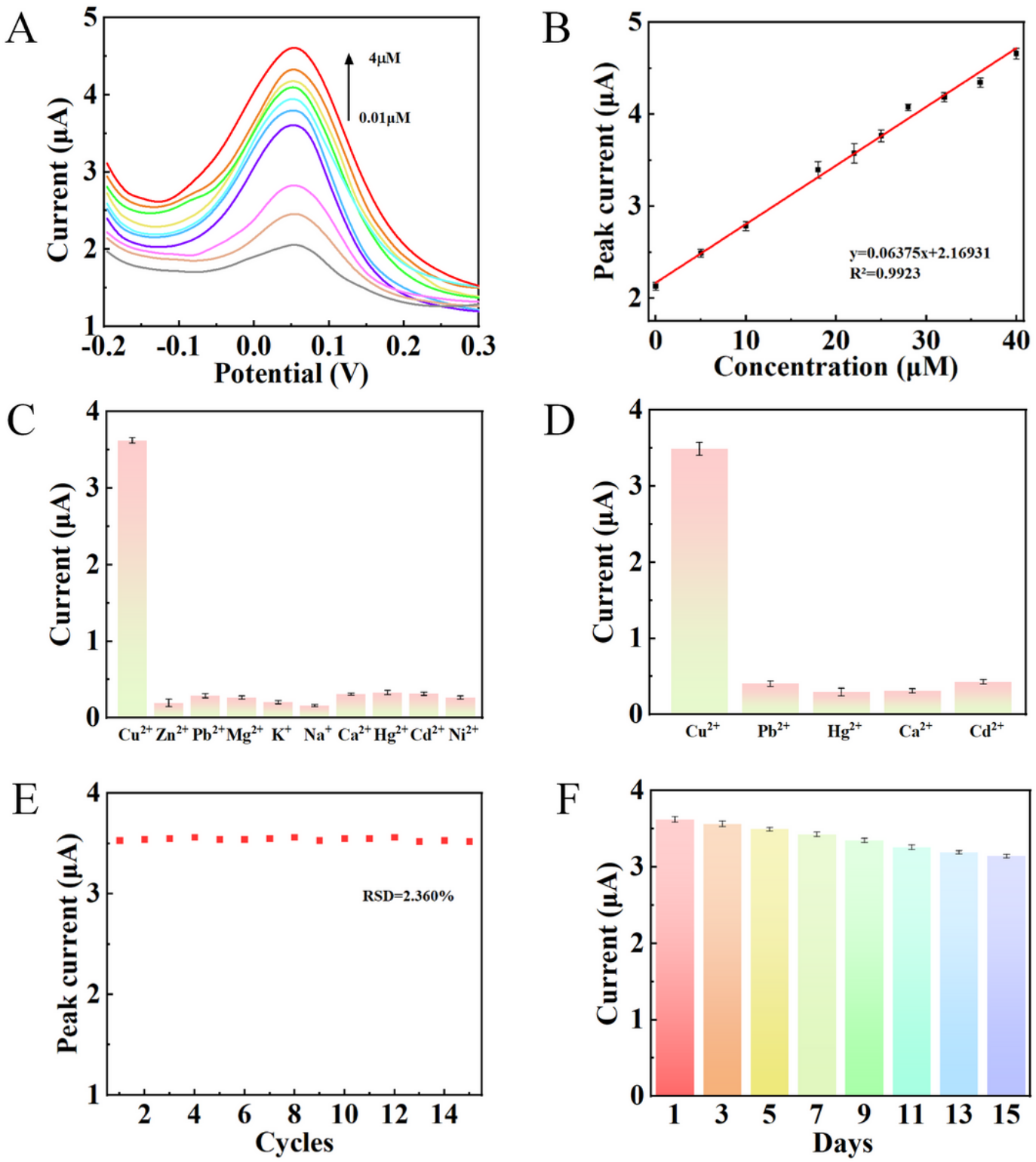

Figure 5

(A) Typical voltammogram of modified SPE as Cu^{2+} concentration increases from 0.01 to 40 μM, (B) Calibration curve for Cu^{2+} detection, (C) Selectivity test of the sensor, Cu^{2+} has a metal ion concentration of 10 μM, other metal ions are 100 μM, and (D) Cu^{2+} (10 μM), other metal ions (1 μM), (E) repeatability study of the sensor, and (F) long-term stability study of the sensor.